ELSEVIER

Chemical Geology 238 (2007) 197–212

CHEMICAL GEOLOGY
INCLUDING
ISOTOPE GEOSCIENCE

www.elsevier.com/locate/chemgeo

High resolution Secondary Ionisation Mass Spectrometry (SIMS) $\delta^{18}O$ analyses of Hulu Cave speleothem at the time of Heinrich Event 1

P.C. Treble [a,b,*], A.K. Schmitt [a], R.L. Edwards [c], K.D. McKeegan [a], T.M. Harrison [a,b], M. Grove [a], H. Cheng [c], Y.J. Wang [d]

[a] *Department of Earth and Space Sciences, University of California Los Angeles, CA 90095-1567, USA*
[b] *Research School of Earth Sciences, The Australian National University, Canberra, ACT 0200, Australia*
[c] *Geology and Geophysics, 310 Pillsbury Dr SE, Minneapolis, MN 55455, USA*
[d] *College of Geography Science, Nanjing Normal University, Nanjing, China*

Received 20 April 2006; received in revised form 15 November 2006; accepted 30 November 2006

Editor: P. Deines

Abstract

The suitability of in situ Secondary Ionisation Mass Spectrometry (SIMS) techniques for measuring O isotopes in speleothems is critically examined by applying this technique to a 500-year interval of the well-known Hulu Cave record (Wang, Y.J., Cheng, H, Edwards, R.L., An, Z.S., Wu, J.Y., Shen, C.C., Dorale, J.A., 2001. A high-resolution absolute dated late Pleistocene monsoon record from Hulu Cave, China. Science, 294: 2345–2348). This interval includes a large abrupt +2‰ shift in $\delta^{18}O$ at 16.07 ka, which may correlate to Heinrich Event I (H1). The high-resolution SIMS method provides annual to near-annual $\delta^{18}O$ data, thereby increasing the temporal resolution of the previously published Hulu Cave isotopic data by approximately tenfold. SIMS $\delta^{18}O$ data reveal that 75% of the abrupt isotopic shift at 16.07 ka occurred in just 1 to 2 years and the full +2‰ occurs over 6 years, compared with an upper limit of 20 years as previously determined by conventional methods employing micro-cutting, acid-digestion and CO_2-gas source mass spectrometry methods. SIMS $\delta^{18}O$ data also reveal numerous high amplitude (1–3‰), high frequency (<20 year) fluctuations not resolvable with conventional data that are recorded in the several hundred years prior to 16.07 ka and may persist after the 16.07 ka event. These fluctuations are interpreted to represent more local rainfall changes while the +2‰ shift represents a rapid change in the underlying $\delta^{18}O$ mean driven by more complex processes that are maintained for 500 years.

Keywords: SIMS; Speleothem; Oxygen isotopes; Heinrich; Ion probe

1. Introduction

1.1. Abrupt climate events during the last glacial

The Earth's climate was remarkably unstable during the last glacial period. The Greenland ice core $\delta^{18}O$ records show repeated and rapid temperature variations of

* Corresponding author. Present address: Research School of Earth Sciences, Building 61, The Australian National University, Canberra ACT 0200, Australia. Tel.: +61 2 6125 4175; fax: +61 2 6125 0738.
E-mail address: pauline.treble@anu.edu.au (P.C. Treble).

0009-2541/$ - see front matter © 2006 Elsevier B.V. All rights reserved.
doi:10.1016/j.chemgeo.2006.11.009

almost the same magnitude of a full glacial–interglacial cycle (Johnsen et al., 1992; Dansgaard et al., 1993; GRIP Members, 1993; Grootes et al., 1993). These fluctuations, known as Dansgaard–Oeschger (D–O) cycles, are asymmetric, have an approximate period of 1500 years and consist of progressively cooler episodes which ultimately terminate in an abrupt warming phase that may have taken place in as little as several decades or less (Dansgaard et al., 1993). The D–O cycles in the ice cores have been linked to pulses of ice rafted debris (IRD) in the Labrador–Irminger Seas (van Kreveld et al., 2000) and the larger less frequent Heinrich events in the north-west Atlantic deep sea cores (Heinrich, 1988; Bond et al., 1992). IRD production from melting icebergs calved from major northern ice sheets during the coldest phase of the D–O cycles are referred to as Heinrich events (Bond et al., 1992). These events are significant owing to the volume of freshwater input into the North Atlantic, which in turn slows or possibly stops the thermohaline circulation (THC) (Broecker, 2003; McManus et al., 2004). Abrupt warming in Greenland accompanies the resumption of the THC and a new D–O cycle begins.

Abrupt climatic shifts coincident with D–O and/or Heinrich events have been identified in records elsewhere. For example, the Atlantic Ocean and its terrestrial margins (Grimm et al., 1993; Cortijo et al., 1995; Wang et al., 2004 and others), Europe (Spötl and Mangini, 2002; Genty et al., 2003), the Pacific Ocean (Hendy and Kennett, 2000), East Asia (An, 2000; Wang et al., 2001; Yuan et al., 2004) and the tropics (Stott et al., 2002; Burns et al., 2003). Establishing the occurrence, timing, duration and relative magnitude of these climatic fluctuations is an important research challenge that will contribute to the understanding of the causes and impacts of these rapid climate fluctuations (see Broecker, 2003).

1.2. Speleothems as recorders of abrupt climate change

Speleothems are proving to be particularly valuable archives of abrupt climate fluctuations (Wang et al., 2001; Spötl and Mangini, 2002; Genty et al., 2003; Wang et al., 2004). Speleothems can be precisely dated by U–Th disequilibrium methods and their widespread geographical distribution offers a way to accurately measure the influence of abrupt climate events across much of the globe.

Speleothems are slow growing (around 20–300 μm/a); however, highly spatially-resolved in situ analyses of oxygen isotopes and trace elements can produce annually to sub-annually resolved climate records (Treble et al., 2003, 2005a). The oxygen isotope signal ($\delta^{18}O$) is an established proxy for investigating climate fluctuations in speleothems. It is sensitive to both the distal activity of the high latitude ice sheets as well as local temperature and rainfall (Hendy and Wilson, 1968). Annually resolved records of speleothem $\delta^{18}O$ would provide unprecedented detail of the climatic behaviour coinciding with North Atlantic events possibly shedding valuable light on the nature of such rapid climate change.

In previous papers, Kolodny et al. (2003), Treble et al. (2005a) and Fairchild et al. (2006) have tested the suitability of the SIMS technique for O isotope analyses of speleothems and demonstrated that the main advantage of this technique is the superior spatial resolution achievable (typically ten-fold or more). The trade-off in using this technique versus conventional methods (i.e. micro-shaving/drilling and CO_2 gas-source mass spectrometry) is the lower precision obtained (e.g. ±0.4–0.7‰ SIMS versus ±0.1‰; 2 s.d.; Treble et al., 2005a). Thus the SIMS technique is most suitable for investigating small time windows in which relatively large isotopic shifts (>1‰) have occurred. In this paper, we apply this technique to a 500-year portion of the well-known Hulu Cave record (Wang et al., 2001) between 16.5 and 16.0 ka. This portion is characterized by an abrupt shift of about 2‰ at 16.07±0.06 ka (Wang et al., 2001; which we shall refer to here as the 16.07 ka event). The $\delta^{18}O$ value after the shift is the highest recorded at Hulu Cave in the last interglacial–glacial–interglacial cycle and is interpreted to represent the driest time window in eastern China during this cycle (Wang et al., 2001). This interval has been correlated with the most recent Heinrich event: H1 (Wang et al., 2001), although the actual relationship between the 16.07 ka isotopic shift recorded at Hulu and H1 is yet to be determined. The higher resolution SIMS $\delta^{18}O$ data reveal detailed information concerning the structure and duration of the abrupt 16.07 ka event recorded in the YT speleothem record. We also describe the analytical technique in greater detail than any of the previous SIMS O-isotope speleothem papers in order to clearly convey the analytical challenges as well as methods we have adopted to try to improve this technique for speleothem measurements.

1.3. SIMS versus conventional techniques

Secondary ionization mass spectrometry (SIMS) analyses remove just over 2 ng of speleothem carbonate by sputtering a crater ~1–2 μm deep. When sequential measurements are made along the growth axis, a spatial resolution of ~20–30 μm is routinely achievable (Kolodny et al., 2003; Treble et al., 2005a; Fairchild

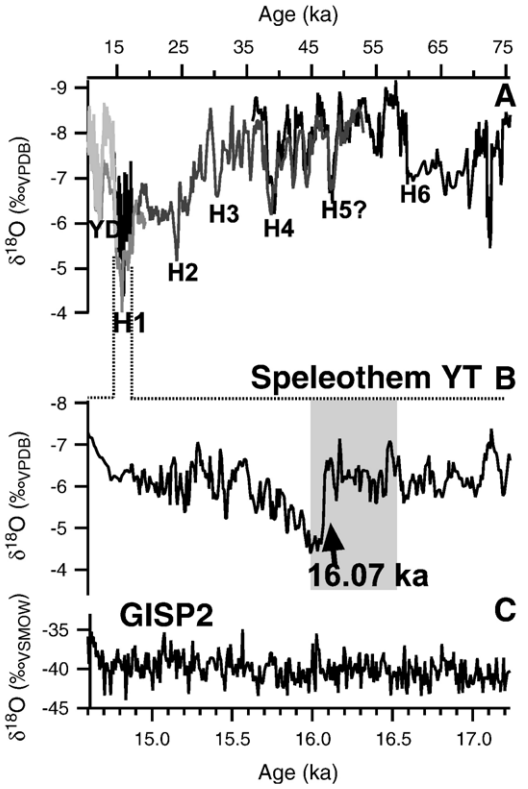

Fig. 1. A–C: Speleothem $\delta^{18}O$ data from Hulu Cave (A–B) and GISP2 data (C; GSIC, 1997). Speleothem data was determined by micro-shaving and conventional acid-digestion methods with five over-lapping records shown (A) and the YT record shown in detail (B) (Wang et al., 2001.) Grey box indicates section replicated with SIMS $\delta^{18}O$ measurements. (Note reversed *Y* axis for speleothems).

et al., 2006). In previous studies, this approach yielded at least yearly (Kolodny et al., 2003) or sub-annual resolution (Treble et al., 2005a), depending on speleothem growth rate. SIMS techniques use far less material compared with techniques that mechanically shave/drill powder for analysis using conventional acid-digestion and measurement by CO_2-gas source mass spectrometry. Not even micro-shaving of carbonate for CO_2-gas source mass spectrometry (e.g. Frappier et al., 2002) can approach the spatial resolution achieved by SIMS, as these other techniques typically shave or file a core that is many times wider in cross-section than the increments sampled along the growth axis. This inevitably smoothes the $\delta^{18}O$ signal, particularly for speleothems whose banding is not perfectly normal to the direction of shaving (e.g. Treble et al., 2005b).

SIMS techniques offer several other advantages over the conventional methods. Their in situ nature permit accurate registration of $\delta^{18}O$ with other in situ measured proxies e.g. trace elements measured by SIMS or laser ablation inductively-coupled mass spectrometry (LA-ICPMS; Treble et al., 2005a). The disadvantage of SIMS $\delta^{18}O$ analyses over conventional techniques is lower precision as mentioned earlier. Acid digestion and CO_2-gas source mass spectrometry routinely achieve $\delta^{18}O$ measurements with an external precision of $<0.1‰$ (e.g. Treble et al., 2005a). For SIMS analyses, it is inherently more difficult to maintain stable running conditions between analyses of standard materials and unknowns, and thus to accurately correct $^{18}O/^{16}O$ measurements for instrumental mass fractionation (IMF). For each new analysis, subtle changes in the surface charge balance and the secondary ion paths may affect IMF. Furthermore, one of the larger hurdles is obtaining standards that are isotopically homogeneous on the spatial scale of the analyses (Kolodny et al., 2003; Treble et al., 2005a). This problem will be examined in more detail in Section 2.

1.4. The Hulu Cave record and the East Asian monsoon

The Hulu Cave record published by Wang et al. (2001) is a composite of $\delta^{18}O$ data from five stalagmites each growing over some 3000 to 40,000 years in duration which together span the interval 75 to 11 ka (Fig. 1A–B). This composite record varies by 5‰ overall and shows six intervals characterized by high $\delta^{18}O$ values (low precipitation), which have been correlated with Heinrich events H1 to H6, which in turn, are correlated with low $\delta^{18}O$ (low temperature) intervals in the Greenland ice core records (GRIP and GISP2). The striking resemblance between the GISP2 and Hulu Cave records overall (see Wang et al., 2001) suggests the Hulu Cave speleothems are robustly recording climate signals.

Hulu Cave is situated 28 km east of Nanjing (32°30′ N, 119°10′ E; Fig. 2) and receives an annual rainfall of 1750 mm. The East Asian region is dominated by two distinct monsoon stages each year with the majority of rain (approximately 85%) falling between May and September (Fig. 3A). The Hulu Cave record is primarily controlled by variations in the East Asian summer monsoon (EASM) (Wang et al., 2001) and also bears close resemblance to the Dongge Cave (1200 km WSW of Hulu) record (Yuan et al., 2004) controlled by both the East Asian and Indian monsoons.

The EASM is driven by the northward migration of the intertropical convergence zone (ITCZ) and the contrast in sea level pressure between the Asian continent and the surrounding oceans. In June, a strong pressure gradient along southeastern China between the continental low pressure cell and the northwestward migration of the

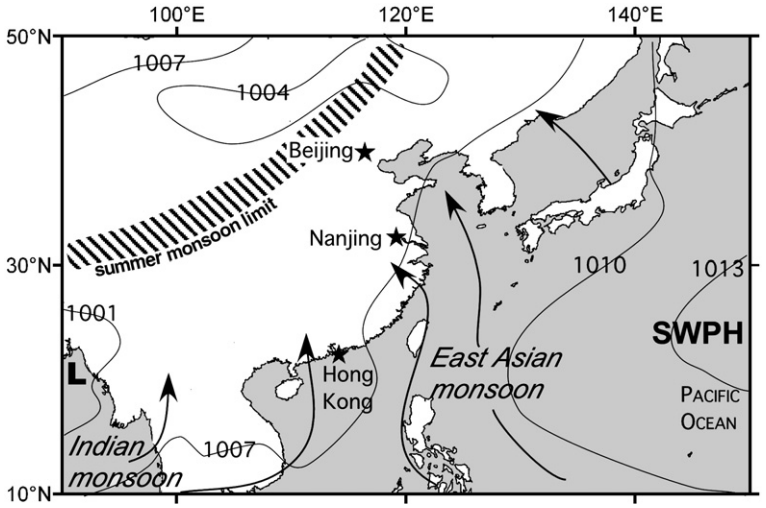

Fig. 2. Location of Hulu Cave, the East Asian summer monsoon (EASM) limit and the subtropical western Pacific high (SWPH). Isobars (interval 3 hPa) indicate mean sea level pressure for June and arrows indicate the flow of moist air from the Pacific and Indian Oceans.

subtropical western Pacific High (SWPH) sets up a conduit of moisture manifesting as the EASM. The moist air originates predominantly over the subtropical western Pacific Ocean but also as far as the Indian Ocean (Domrös and Gongbing, 1988; Lim et al., 2002; Fig. 2). The resulting monsoonal rainfall is isotopically depleted ($-9‰_{VSMOW}$, Fig. 3B; Araguas-Araguas et al., 1998). From about mid-July onwards, the SWPH decays and a vast area of low pressure develops over the subtropical western Pacific merging with low pressure across the continent, diminishing the flow of moisture from the Indian Ocean (Lim et al., 2002). Rainfall over eastern China continues to be sustained by convective activity within this low-pressure zone, sourcing moisture from the sub-tropical Pacific Ocean until late August. The airflow over eastern China reverses to a northeasterly flow after August, when a high pressure cell evolves over the cooling continent and low pressure cyclonic circulation to the east over the Pacific is maintained (Lim et al., 2002). Much smaller amounts of relatively ^{18}O-enriched rainfall occurs throughout September to March (Fig. 3A, B). Distinctly higher deuterium excess (d_o) values (Fig. 3C) indicate moisture is sourced under different conditions during these months and a change to local western Pacific sources has been suggested (Araguas-Araguas et al., 1998).

Wang et al. (2001) interpret the sudden shifts to more positive $\delta^{18}O$ values in the Hulu Cave record that coincide with North Atlantic Heinrich events as evidence for a weakening of the EASM. The shift to high $\delta^{18}O$ at 16.07 ka correlated with H1 is one of the most prominent in the record and is replicated in three of the Hulu Cave stalagmite records. The fastest growing of these is stalagmite YT which is 11.5 cm tall and grew between 17.2 and 14.4 ka. The abrupt 2‰ ^{18}O-enrichment coinciding with H1 occurs at 16.07±0.06 ka and mean $\delta^{18}O$ does not recover to prior values until 15.6 ka (Fig. 1B) according to the chronology defined by three U–Th disequilibrium age determinations (14.61±0.07, 15.91±0.06, 17.16±0.09 ka; 2σ) and annual band counting (Wang et al., 2001). Micro-shaved intervals carried out for conventional $\delta^{18}O$ analyses across this interval represent approximately 4 years of growth, however, as analyses were only carried out on alternate samples, the effective resolution is about a decade.

2. Methods

2.1. SIMS O isotope analyses

SIMS $^{18}O/^{16}O$ measurements were carried out on a Cameca IMS1270 instrument at the University of California, Los Angeles. The spatial resolution of SIMS sputter craters about 30 μm wide, approximating the relatively constant annual growth rate of speleothem YT indicated by annual band counting (Y.J. Wang, unpublished data). In order to yield annually-resolved transects of $\delta^{18}O$ data along the central growth axis of speleothem YT, sequential analyses were offset in a zig-zag fashion to maintain at least 20 μm of Au coating around each new measurement spot (see Fig. 3 in Treble et al., 2005a) to ensure electrical conductivity. As visible banding in speleothem YT is near-parallel and horizontal across the measurement section, we believe that these small lateral offsets do not affect the quality of the data. Owing to its slow growth, it is not known whether speleothem YT

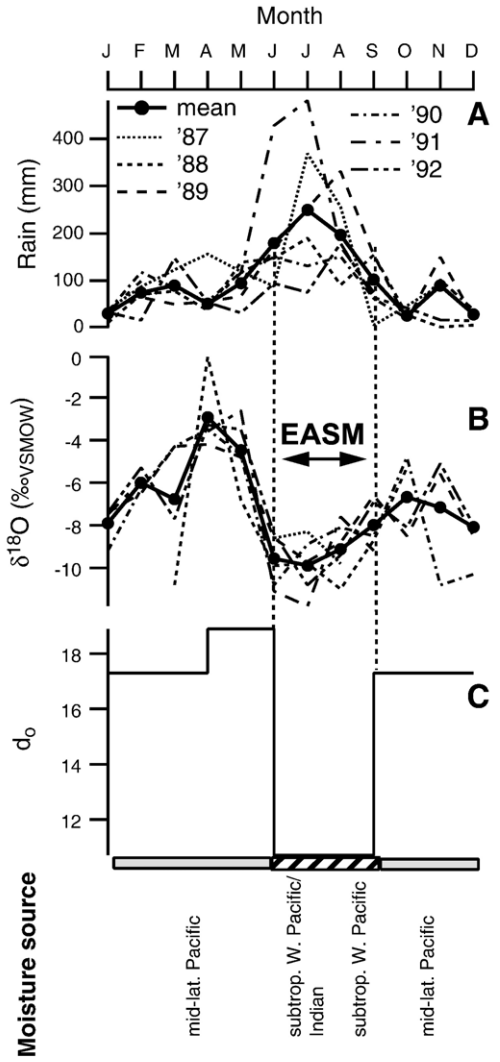

Fig. 3. Monthly rainfall amount (A), monthly rainfall $\delta^{18}O$ (B) and seasonal deuterium excess, d_o, at Nanjing (1987–1992, incomplete; IAEA/WMO, 2001). Heavy lines in A and B are monthly means while d_o (C) is the mean of each of the three monsoon intervals (April–May, June–August, September–March). Monsoon moisture sources (Lim et al., 2002) are indicated at bottom. Rainfall $\delta^{18}O$ is lowest during the wettest period, the East Asian summer monsoon (EASM), when moisture is drawn by low-level winds from the sub-tropical Pacific Oceans and possibly as far away as the Indian Ocean.

preserves the seasonal range of rainfall $\delta^{18}O$ or if this signal is smoothed in the overlying limestone. In either case, consistently spaced analysis spots that approximate the near-constant annual growth increments over the measured section, assuming intra-annual growth variations are not large, should yield $\delta^{18}O$ measurements that approximate mean annual $\delta^{18}O$.

Thermally generated $^{133}Cs^+$ ions were accelerated to 20 keV towards the sample surface. A defocused $^{133}Cs^+$ primary beam was projected onto a 100 μm aperture to obtain a homogeneous beam with a ~5 nA current focused onto the sample surface in a 30 μm spot. On calcite, this beam excavates a crater at a rate of ~1.2 μm^3/nA/s and the atoms removed become partially ionized. Negative secondary ions are then accelerated at 10 keV and transmitted into a double focusing mass spectrometer via a series of transmission lenses and deflectors which help to keep the secondary ion path constant with regard to spectrometer admittance. A combination of continual implantation of positive $^{133}Cs^+$ ions while removing secondary ions and electrons leads to rapid and substantial charge build-up (Ireland, 1995). This charge is partially dissipated by Au coating of the sample surface and more effectively by neutralization via a normal incidence electron gun which generates a cloud of electrons approximately three times the diameter of the ion crater.

Following beam dispersion within an electrostatic analyzer (ESA), secondary ions with energies between ~0 and 30 eV excess energies are separated with a magnetic field set to an axial mass/charge (m/c) value of ~17 amu. Hydride ($^{16}O^1H$) ions with m/c=17.0027 amu are projected onto an axial channel plate, yielding an ion image of the sample surface which is used for the adjustment of secondary ion admittance within the so-called field aperture located upstream of the ESA. Oxygen ions with m/c=15.9994 and 17.9992 amu are diverted via individual ESA's into two Faraday cups for simultaneous multiple collection. A pair of slits allow separation of oxygen ions at a mass resolving power of ~2400 from hydride interferences such as m/c=18.0106 ($H_2^{16}O$).

Prior to secondary ion counting, the $^{16}OH^-$ image was centred in the partially closed field aperture (3 mm) by adjusting deflectors for *x*- and *y*-steering of secondary ions whenever sequential analysis spots were more than 0.25 mm apart, i.e. moving between unknown and standard. The pre-sputter time was electronically monitored and after exactly 180 s the analysis was started. During analysis, the field aperture was kept wide open (7.5 mm) permitting all sputtered ions in the sputtered spot to pass through. $^{18}O^-$ and $^{16}O^-$ ion beams were collected simultaneously in Faraday cups for 100 s (collected in 10 blocks of 10 s integration time). Primary beam stability was sufficient throughout each session (±5%) to keep secondary ion intensities within a narrow range which avoided the potential need to correct for non-linear detector response. During set-up, strong variations in secondary ion intensity that correlated with shifts in $\delta^{18}O$ values were occasionally detected and any such data were discarded and secondary ion tuning re-examined.

Table 1
Statistical summary of standards NBS19 and SRM612 for each analytical session (values given in ‰ are VSMOW)

Session	Unknown analyses	Standard analyses	Mean IMF [a] (‰)	Total drift [b] (‰)	Internal error [c] 1σ (‰)	External precision [d] ±2 s.d. (‰)	NBS18 cross calibrated value [e] ±1σ (‰)
1.1	77	20 (NBS19)	−6.9	<1.5	0.07	±0.9	6.5±0.12 [4]
1.2	118	23 (NBS19)	+0.7	<3.0	0.10	±1.5	7.1±0.14 [7]
1.3	126	27 (NBS19)	−7.2	<2.0	0.11	±1.3	7.8±0.15 [5]
2.1	221	102 (SRM612)	+0.4	1.6	0.06	±0.4	
		16 (NBS19)	−1.9	<2.7	0.06	±1.2	7.6±0.08 [10]
3.1	50	23 (SRM612)	+4.1	0.6	0.06	±0.5	
		10 (NBS19)	−0.4	<2.5	0.05	±1.8	5.9±0.07 [10]
4.1	101	52 (SRM612)	−7.0	7.7	0.07	±5.1	
		10 (NBS19)	+0.4	1.0	0.07	±0.5	8.3±0.09 [10]

For NBS19 and SRM612, we adopt ±2 standard deviation (s.d.), rather than standard error (σ), as an estimate of external precision as we are interested in point-to-point reproducibility rather than the mean.
[a] Calculated as $(^{18}O/^{16}O_{measured} - ^{18}O/^{16}O_{true})/^{18}O/^{16}O_{true} \times 1000$.
[b] Could not be calculated for NBS19 due to large uncertainty. Value given is range of measurements.
[c] Mean of internal error of analyses determined from counting statistics.
[d] Calculated as ±2× the standard deviation (s.d.) from the mean of standards measured in each session. For 2.1, 3.1 and 4.1 these were calculated before (values in brackets) and after correcting for IMF drift (not bracketed).
[e] NBS18 accepted value is +7.2‰$_{VSMOW}$. ±1σ error calculated by adding NBS19 and 18 internal errors in quadrature.

Under these conditions, ^{16}O (^{18}O) count rates are achieved on the order of $\sim 5\times10^9$ cps (1×10^7 cps), which correspond to a useable O yield of ~4%. Internal precision is not limited by counting statistics since there is sufficient O in carbonates to obtain a counting error of 0.1‰ or less (1σ) over 100 s of integration time. It is, however, commonly observed that variations in isotopic ratios determined from repeat analyses are significantly larger than predicted from the internal precision. A key factor which largely determines the reproducibility of SIMS isotope analyses is therefore achieving constant IMF. The largest source of IMF is related to ionization efficiency close to the sample surface (Ireland, 1995; Valley et al., 1998). For example, charge compensation within the sputter-crater can be disrupted by cracks in the sample or gaps between the sample and mounting medium that affect local electrical continuity surrounding the analytical area (Valley and Graham, 1991). Subtle sample topography, especially near the edges of the front plate of the sample holder, and constant ambient magnetic fields also influence ion trajectories and can result in a non-uniform isotope distribution within the secondary beam (Schuhmacher and de Chambost, 2004).

2.2. Standardisation

Standard materials are included to correct for IMF in measurements of unknowns and to monitor the reproducibility of isotopic measurements under conditions that are equivalent to those for the unknowns. Ideally, suitable standards are identical in mineral composition to the unknowns producing the same ion yield. Obtaining calcites that are isotopically homogeneous at the 30 μm spatial scale is one of the largest difficulties in successfully referencing SIMS O isotope analyses against an absolute scale such as Vienna Standard Mean Ocean Water (VSMOW) or Vienna Pee Dee Belemnite (VPDB), and has also been shown to represent a significant limitation for a reliable determination of the external reproducibility (Valley et al., 1998). For example, optical calcite (OC) was used in earlier studies as an external standard at the University of California at Los Angeles (UCLA) and Kolodny et al. (2003) adopted this standard in their SIMS $\delta^{18}O$ analyses of Soreq Cave (Middle East) speleothems. However, in the course of their study, Kolodny et al. (2003) determined by CO_2-gas source mass spectrometer techniques that sub-samples of standard OC differed by 1‰ owing to isotopic zoning in the crystal. Kolodny et al. corrected the speleothem SIMS analyses to values determined by CO_2-gas source mass spectrometry analyses at discrete points. Here and in a previous study (Treble et al., 2005a), it was found that SIMS analyses of National Institute of Standards (NIST) NBS18 and NBS19 carbonate standards yielded an external variability that was typically ~2 to 7 times larger than found on NIST SRM612 glass during the same analytical sessions. While this does not conclusively prove μm-scale oxygen isotopic heterogeneity of these carbonate standards, these findings clearly indicate the need for further

characterization and development of calcite standards for microanalysis.

Analyses were conducted over six collection sessions denoted by 'X.x' where 'X' refers to the measurement block which is subdivided into sequential measurement sessions 'x' (typically one day). For example, sessions 1.1, 1.2 and 1.3 refer to three sequential measurement days. Analytical conditions are maintained between sequential sessions with only minor adjustments made to the primary beam intensity, Faraday Cup trolley alignment and secondary tuning. Between a block of measurement sessions, ion microprobe primary and secondary ion polarities and tuning conditions were modified, and therefore the analytical set-up between blocks of sessions where oxygen isotopes were analyzed may have differed markedly.

Standards NBS18 and 19 were used during sessions 1.1–1.3 but it was realized that an isotopically homogeneous standard was needed to better monitor IMF drift and that natural carbonates appeared to be inherently heterogeneous. Thus, SRM612 silicate glass ($\delta^{18}O = +10.3‰_{VSMOW}$; Kasemann et al., 2001) was employed as an internal standard (sessions 2.1, 3.1 and 4.1). Repeat analyses of SRM612 yielded an external precision of ±0.5‰ (2 s.d.; Table 1) or less except for session 4.1 discussed later. In addition, SRM612 has a similar O ion yield (^{16}O: 4×10^9 cps; ^{18}O: 8×10^6 cps) and could be cut into fine strips and mounted adjacent to the speleothem therefore minimising travel distance between sample and standard and could also be polished flat. We also mounted NBS19 and NBS18 grains on the same mount to obtain a mean IMF correction value between the glass and carbonate standard materials that could be applied to the speleothem $^{18}O/^{16}O$ measurements.

For sessions 2.1, 3.1 and 4.1, every five speleothem measurements were bracketed by one background measurement and two measurements of SRM612 standard material. Between 4 and 10 measurements each of NBS18 and NBS19 were included in each measurement session to measure the difference in IMF between calcite and silicate glass (Table 1). Systematic drift in SRM612 $\delta^{18}O$ measurements greater than 0.5‰ were removed from the SRM612 and speleothem $^{18}O/^{16}O$ measurements by subtracting linear interpolations through intervals of data affected by the drift (shown graphically later).

IMF drift corrected speleothem $^{18}O/^{16}O$ measurements were corrected to mean NBS19 values by multiplying $^{18}O/^{16}O$ speleothem by the ratio $(^{18}O/^{16}O_{true})/(^{18}O/^{16}O_{measured})$ determined from the mean of each session and expressing $^{18}O/^{16}O$ in delta notation relative to VSMOW (Eq. (1)).

$$\delta^{18}O_x = \left(\frac{^{18}O/\ ^{16}O_x}{^{18}O/\ ^{16}O_{VSMOW}} - 1\right) \times 1000 \quad (1)$$

and converted to VPDB using the relationship (Coplen, 1988):

$$\delta^{18}O_{VPDB} = 0.97001 \times \delta^{18}O_{VSMOW} - 29.99 \quad (2)$$

2.3. Sample preparation

A thin slice of speleothem approximately 2–3 mm wide was cut from the central growth axis of speleothem YT and gently snapped rather than cut in order to avoid measurement gaps. The calcite fragments, approximately 15 mm long are mounted closely together with similar sized strips of SRM612 as well as NBS19 and NBS18 grains into 2.5 cm diameter epoxy resin disks. The carbonates, glass and epoxy are carefully flattened by wet polishing. Smooth featureless speleothem calcite is ideal for SIMS analyses (e.g. completely fused columnar palisade calcite; Kendall and Broughton, 1978) to maintain consistent electrical conductivity across the surface. Inclusion-rich calcite and micro-crystalline calcite that is easily plucked during polishing, leaving a pitted surface, should be avoided.

2.4. Speleothem Mg measurements

Mg concentrations were measured across the transect of SIMS analyses by LA-ICPMS at the Australian National University following the method described in Treble et al. (2003, 2005a). The laser was masked to create a 5×50 μm ablation area, thus obtaining 5 μm resolution in the direction of the growth axis.

3. Results

3.1. Geometry effects

The main advantage of the sample design described is that SRM612 can be used to monitor IMF variations that result from variability in secondary ion extraction and steering due to the geometry of the sample holder, known as geometry effects (e.g. Valley and Graham, 1991). Routinely, the secondary ion path was realigned prior to the analysis by using a pair of *x* and *y* deflectors by centering the secondary ion image in the field

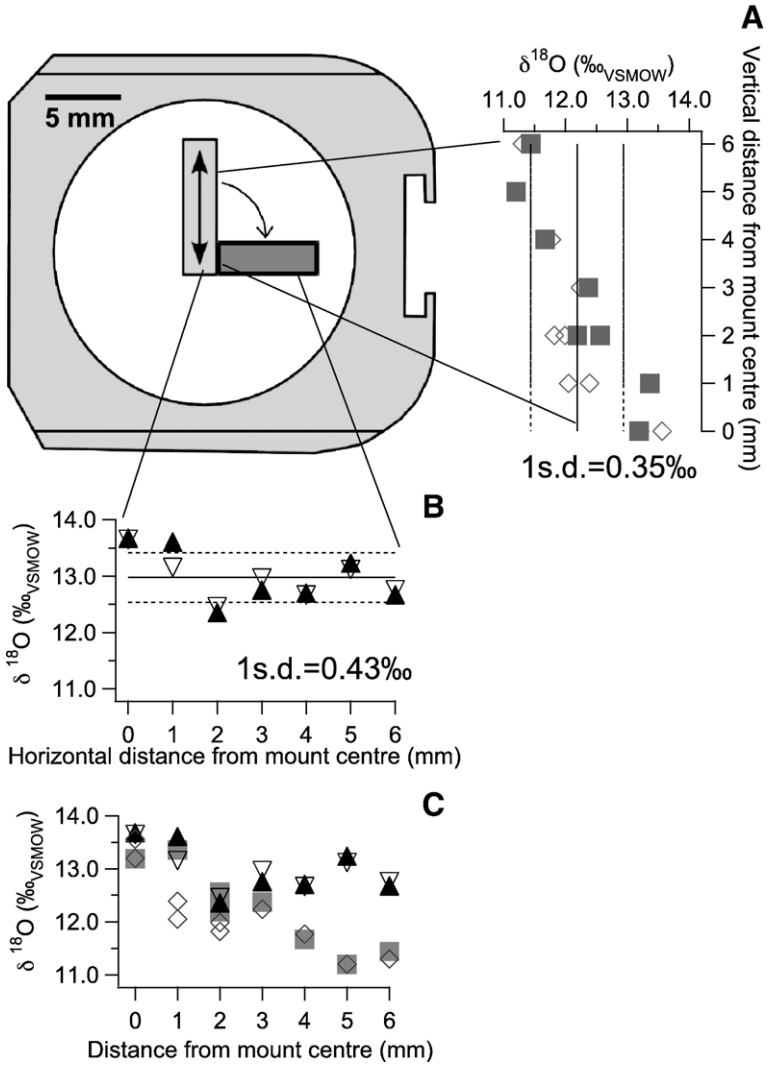

Fig. 4. Repeat $\delta^{18}O$ measurements of SRM612 along the same transect between 0 and 6 mm from the mount centre with the mount orientated vertically (A) and horizontally (B) in the sample holder. Closed symbols are the forward and open symbols are the reverse transect for each orientation and dashed lines indicate ±1 s.d. from the mean of each dataset. Agreement between forward and reverse transects within each orientation is very good (less than 0.5‰ except at 1 and 2 mm vertical orientation) but agreement between vertical and horizontal transects is poor particularly towards the mount edge where values differ by up to 2‰ (C). This indicates that geometric induced IMF is affecting the values since measurements at each 1 mm interval are essentially repeat measurements at the same point on SRM612.

aperture. In addition, the centering of the secondary beam within the entrance slit was checked after major primary beam adjustments became necessary (e.g., between sessions 2.1 and 3.1). However, it was felt that these measures were insufficient to completely compensate for geometry effects. Fig. 4 shows results for an experiment during which replicate transects, each containing between 14 and 17 measurements between 0 and 6 mm from the centre of the mount, were obtained. Measurements were first obtained along a transect 0–6 mm and then repeated by retracing the transect back to the mount centre (6–0 mm) with the SRM612 strip orientated vertically (Fig. 4A). The mount was then removed and rotated 90° and the experiment repeated at the same intervals on the glass but with the glass mounted horizontally (Fig. 4B). The resulting 4 analyses at each 1 mm step are located within approximately 100 μm of each other. Thus the measurements are made at essentially the same point on the glass but with the orientation of the glass first vertical and then horizontal.

$\delta^{18}O$ values are well reproduced and are not more than 0.5‰ apart between each forward and retreat

transect for each orientation, except at 1 mm (vertical orientation) where the $\delta^{18}O$ value was 1‰ higher on the forward transect compared with duplicate measurements made on the retreat transect. However, considering the dataset overall, one standard deviation of 30 replicate analyses over the 6 mm covered by the transects is 0.74‰ and $\delta^{18}O$ values decrease towards the mount edge. $\delta^{18}O$ values measured in the vertical orientation are consistently between 0.5 and 2‰ lower than values measured at the same location in the horizontal orientation with greater disagreement towards the mount edge (Fig. 4C). Isotopic heterogeneity can be ruled out since each group of measurements are within 100 μm of each other and forward and retreat paired measurements within each orientation typically agree to within 0.5‰. No time-dependent drift in IMF is evident either. The reproducible variations between forward and retreat transects at each orientation lead us to conclude that shifts in IMF on SRM612 are dependent on sample geometry and become larger further from the mount centre. Possible reasons for this are divergence of the secondary ion beam from the ion optical axis due to stronger deflection values or compromised charge compensation due to deflection of the electron cloud away from the mount center.

Whatever the reason for these geometry effects, our mounting technique of arranging strips of SRM612 directly adjacent to the speleothem strip, minimizing travel distance to approximately 500 μm ensures that geometry (as well as time induced) IMF can be monitored throughout the speleothem measurement transect.

3.2. External precision of analyses

Carbonate standards were initially analyzed to determine point-to-point external reproducibility and to monitor IMF throughout each session. A statistical summary of standard measurements in individual sessions is summarized in Table 1. For sessions 1.1–1.3, speleothem YT measurements were standardized to the mean of NBS19 grains. The variability in NBS19 measurements was too large (±0.9–1.5‰, 2 s.d.; Table 1) to determine whether IMF drift was present over long periods. Variability of repeat measurements of NBS19 is also poor (±1.2–1.8‰, 2 s.d.) when measured against SRM612 (±0.4–0.5‰, 2 s.d.; sessions 2.1 and 3.1; Table 1). This confirms earlier suggestions by Treble et al. (2005a) that the uncertainty associated with measurements of the carbonate standards are due to properties inherent to the grains rather than IMF. Treble et al. suggested this variability could be due to either isotopic heterogeneity or subtle topography created during polishing small grains. The other carbonate standard, NBS18, was treated as an unknown throughout all sessions and its mean value (excluding session 4.1; $+7.0‰_{VSMOW}$) is very close to the accepted value ($+7.2‰_{VSMOW}$). The agreement between the overall mean of the NBS18 data with the accepted value suggests that the variability in these carbonate standard measurements is due to isotopic heterogeneity within and between grains as the same grains were not targeted in each session.

We will now consider the analytical precision of the speleothem data by examining SRM612 values through each session. Sessions 2.1 and 3.1 are repeats of sessions 1.1 and 1.2 with SRM612 included. We attempted to similarly re-measure speleothem $\delta^{18}O$ data acquired during session 1.3 during session 4.1 but this data will not be discussed owing to instrumental instability throughout the measurement session where sudden changes in instrumental stability produced shifts of up to 5.5‰ between analyses and SRM612 varied by up to 7.7‰ overall (Table 1). These variations were too large to be confidently corrected for by subtracting drift in SRM612 values as described. Much smaller systematic drift is present throughout sessions 2.1 and 3.1. Drift persisting over long periods is shown for session 2.1 (Fig. 5A–C) where for example, SRM612 $\delta^{18}O$ values decrease by 0.9‰ over a 6 h period between analyses 130–175 (Fig. 5C) while each pair of SRM612 measurements consistently differ by no more than 0.5‰. The long-term drift in SRM612 measurements is not due to isotopic heterogeneity of the glass as sessions 2.1 and 3.1 measurements overlap on the SRM612 glass and do not produce the same trends. Rather this drift is due to either the geometry effects described in Section 2.2 or time-dependent instrumental stability or some combination of the two. For either case, mounting SRM612 in a strip directly next to the speleothem allows us to monitor and subtract this drift from the analyses. The external precision of SRM612 in session 2.1 after such drift is removed is ±0.4‰ (2s.d.; Table 1) compared with ±0.8‰ (2 s.d.) beforehand. This corrected value is closer to the mean difference between each paired measurement ($\leq$0.5‰) indicating that we are able to correct for almost all of the uncertainty created by variations in IMF. Moreover, the agreement between overlapping SIMS transects as well as the agreement between mean trends (but not absolute values) in SIMS and micro-shaved data (discussed further in Section 3.2) indicate that this method is appropriate.

SRM612 can be used to estimate the external reproducibility of analyses but not accuracy owing to the dissimilarities between the glass and speleothem

materials. To express speleothem measurements with respect to the VSMOW or VPDB scale, the speleothem $^{18}O/^{16}O$ ratios were ultimately corrected for instrumental mass fractionation determined on NBS19. The accuracy of this correction is dominated by the uncertainty in NBS19 measurements (Table 1) and potentially, variations in glass-calcite fractionation between glass-NBS19 measurements (which were

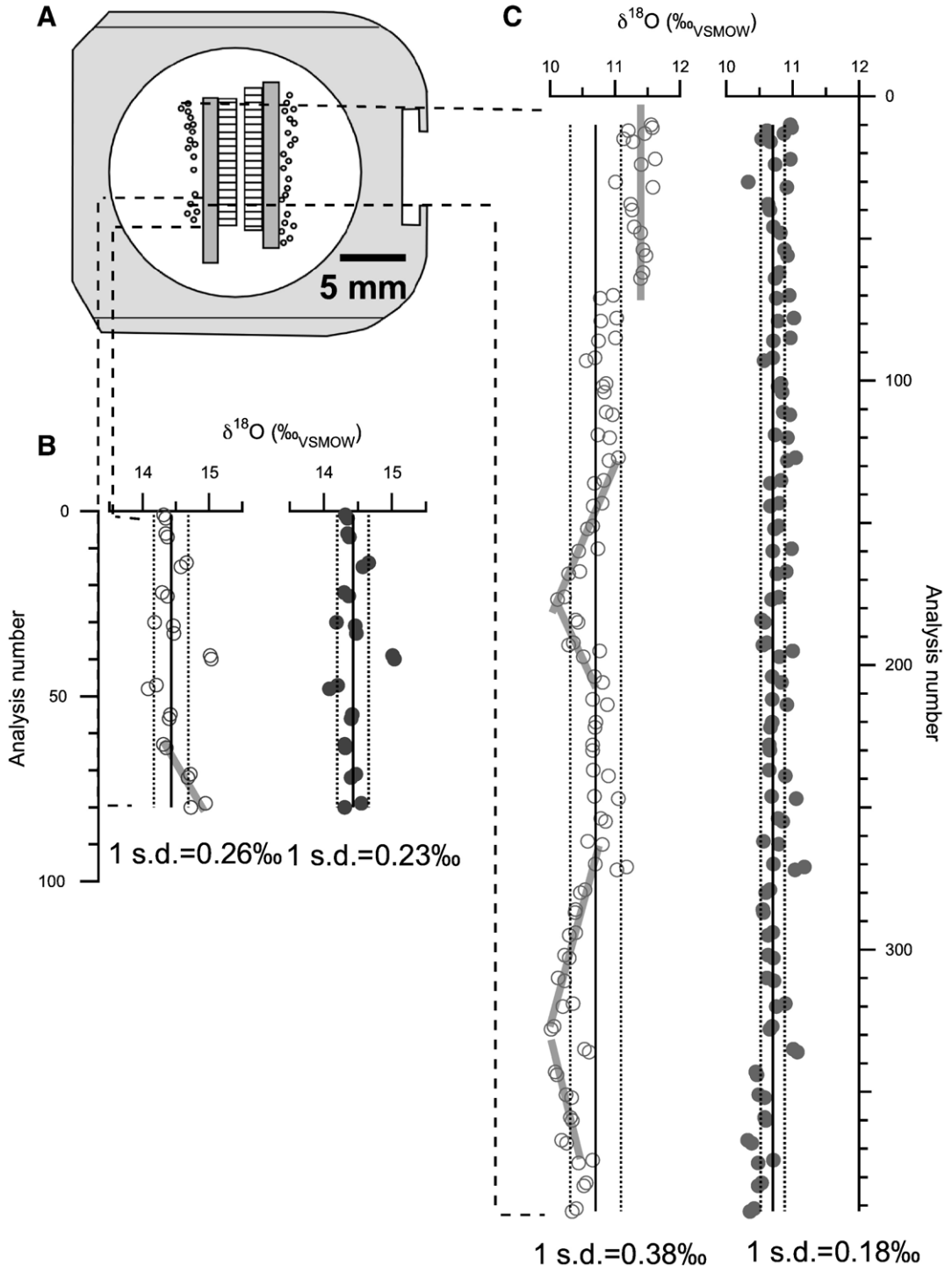

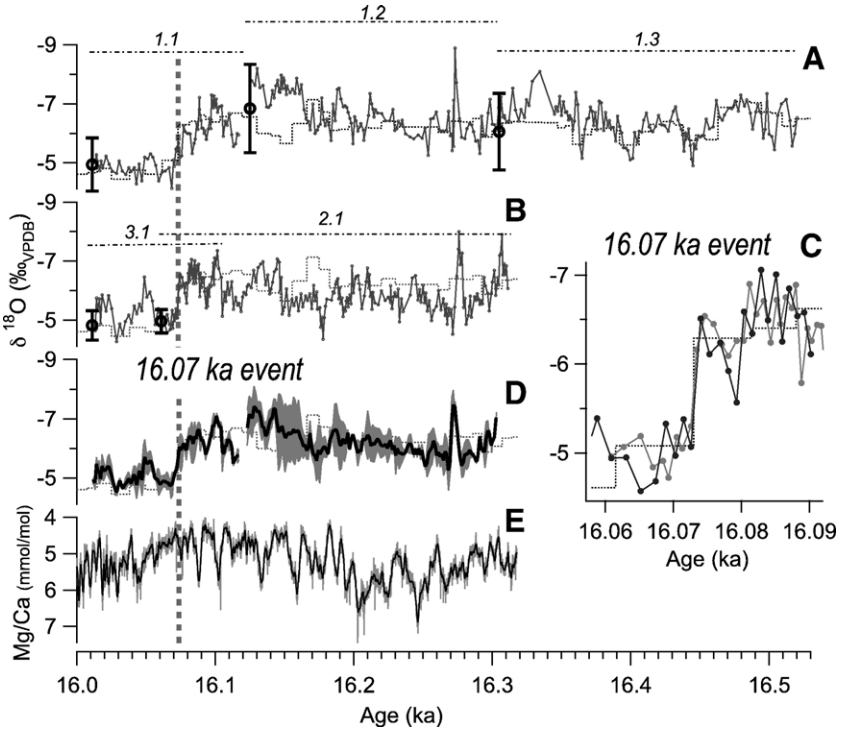

Fig. 6. A–E: SIMS data compared with micro-shaved data of Wang et al. (2001) (A–D) and speleothem Mg (E). (A) Sessions 1.1–1.3 and (B) sessions 2.1 and 3.1 SIMS $\delta^{18}O$ data. Single error bars on the final point of each session are ±2 s.d. calculated from repeat measurements of either NBS19 (A) or SRM612 (B). ±2 s.d. represents 95% of the variability of standard measurements and is an appropriate estimate of point-to-point reproducibility available for each session. Error bars for sessions 1.1–1.3 are ±2 s.d. of NBS19 (±0.9–1.5‰) which is likely to be larger than the speleothem data owing to the isotopic heterogeneity of NBS19. Subsequent measurements on isotopically homogeneous SRM612 (sessions 2.1 and 3.1) produce a smaller estimate of point-to-point reproducibility (±0.5‰ or less; 2 s.d.). Overlapping SIMS transects from sessions 2.1 and 3.1 highlight the rapid 1–2 year isotopic shift at 16.07 ka (C). Combined SIMS data (D) indicates the overall agreement between multiple transects and show excellent agreement over other sections such as the 3‰ excursion at 16.27 ka (grey envelope indicates the range of measurements and dark line indicates the mean). Similar features are recorded between 1.1 and 3.1 but are offset by ~0.5–1‰. Mean speleothem Mg, indicated by dark line is 11-point box smoothed data (E). (Note Mg and $\delta^{18}O$ scale inverted.)

conducted either at the beginning or the end of a speleothem measurement session) and glass-speleothem measurements. Hence there are minor residual offsets between mean trends of YT micro-shaved and SIMS $\delta^{18}O$ data. For compensation of this residual bias, and to facilitate visual comparison, SIMS $\delta^{18}O$ YT data were shifted by +0.5‰ (1.1), +1.0‰ (1.2), −0.5‰ (1.3), and +1.0‰ (2.1 and 3.1) which approximately aligns them with the mean of the micro-shaved data over corresponding intervals (Fig. 6A, B).

3.3. Comparing in situ (SIMS $\delta^{18}O$ and Mg) and micro-shaved $\delta^{18}O$ data

Comparing broad trends, the agreement between micro-shaved and SIMS $\delta^{18}O$ data is particularly good for session 1.1 (16.12–16.01 ka) and session 1.3 between 16.52 and 16.36 ka, with the 16.07 ka event as well as four large cycles, each 30 to 60 years duration (16.52–16.36 ka) clearly reproduced in greater detail (Fig. 6A). But agreement is less clear for session 1.2,

Fig. 5. Sketch of sample mount with speleothem YT and standards (A). Speleothem YT is mounted in two strips in the centre of the mount, bracketed by two strips of SRM612. NBS19 (right) and NBS18 (left) grains are mounted either side of SRM612. Background-corrected (open circles) and drift corrected (filled circles) raw $\delta^{18}O$ measurements for SRM612 in session 3.1 (B) and 2.1 (C). Dashed lines indicate ±1 s.d. from the mean of each dataset. Paired analyses on SRM612 were made every 5 speleothem measurements. For each SRM612 pair, $\delta^{18}O$ values differ by no more than 0.5‰ and typically 0.2‰ or less. Instrumental fractionation owing to geometric and time dependent drift between paired SRM612 measurements changed by up to 0.5‰ for analysis time intervals of approximately 1 h, and up to 0.9‰ over 6 h periods (analysis number 130–175). Drift corrections were made if variations exceeded 0.5‰ between SRM612 measurement pairs (intervals indicated by thick grey lines). This was done by adjusting the mean between analyses 0 and 64 and for other indicated sections, by subtracting a linear fit.

particularly over the interval 16.20 and 16.12 ka, where SIMS and micro-shaved $\delta^{18}O$ trends are antipathetic and mean values differ by up to 1.5‰. Session 2.1 SIMS data shows similar variation to that of session 1.2 including over the interval 16.20–16.12 ka where data from neither session agree with the micro-shaved data (Fig. 6A,B). Within this interval, SIMS measurements from both sessions show $\delta^{18}O$ values that are 1‰ more negative between 16.15 and 16.12 ka and 0.5–1.0‰ more positive between 16.20 and 16.15 ka which is antiphase to the micro-shaved data trends. A 3‰ excursion appears in both sessions 1.2 and 2.1 at 16.27 ka and mean $\delta^{18}O$ varies by about 2‰ between 16.32 and 16.22 ka for sessions 2.1, 1.2 and 1.3 (Fig. 6A,B) while the micro-shaved data are largely unchanged through this period. Sessions 1.1 and 3.1 differ by about 0.5‰ after the 16.07 ka event. Given that the mean trend through session 1.1 agrees well with the micro-shaved data, this suggests the mean correction applied to session 3.1 may be up to 1.0‰ too low. On the other hand, further adjusting data from session 3.1 would reduce the agreement between SIMS $\delta^{18}O$ data and micro-shaved data over the interval during which sessions 3.1 and 2.1 overlap (Fig. 6B).

The agreement between sessions 1.1, 2.1 and 3.1 SIMS data, which straddle the 16.07 ka event is extremely good, particularly for sessions 2.1 and 3.1 (Fig. 6B–D). All show an abrupt ^{18}O-enrichment at 16.07 ka and very close similarities in structure before and after, and their mean trend also agrees well with the micro-shaved data. All measurements suggest $\delta^{18}O$ became 2‰ more positive during the 16.07 ka event. However, the far more detailed SIMS analyses reveal that the 16.07 ka event took place in approximately 6 years, which is substantially better constrained than the approximately 20-year value determined from the micro-shaved data. Moreover, the more precise and well-reproduced data from sessions 2.1 and 3.1 suggest this event is dominated by a +1.5‰ transition between three data points in session 2.1 and between two data points in session 3.1 i.e. in just 1–2 years.

The agreement between sessions 2.1 and 3.1 prior to the 16.07 ka event is also extremely good. These data suggest $\delta^{18}O$ varied by more than 1‰ on decadal timescales prior to the isotopic shift at 16.07 ka. After the 16.07 ka event, sessions 1.1 and 3.1 agree in detail but their mean values are approximately +0.5‰ more ^{18}O-depleted than the micro-shaved data. The similar isotopic variation between SIMS sessions suggests the 1‰ ^{18}O-depletion over 16.07–16.05 ka and then gradual ^{18}O-enrichment at 16.03 ka are true variations in the YT record that are not represented in the micro-shaved data. Overlapping SIMS data are combined in Fig. 6D using an envelope to summarise the range of SIMS measurements compared with the micro-shaved data. The heavy line indicates the mean value of the SIMS sessions.

Speleothem Mg/Ca ratios show a broadly positive trend with $\delta^{18}O$ (Fig. 6E). Mean speleothem Mg/Ca is relatively higher after the 16.07 ka event but not as high as it was during 16.32–16.2 ka. Fig. 6E demonstrates that speleothem YT records rapid shifts (2–5 years) in drip water Mg at many times in the record but there is no abrupt shift in speleothem Mg coinciding with the 16.07 ka event, but rather a slow, small rise until about 16.04 ka. Similar to the SIMS $\delta^{18}O$, Mg fluctuates with wavelengths of around 20 years or less, although the timing of these fluctuations coincide only occasionally e.g. 16.27–16.22 ka and 16.14–16.07 ka (Fig. 6D, E). Possible reasons for the phase variation are different lag times of each variable and/or that neither variable is a straight-forward wet/dry signal. There is no distinct change in Mg coinciding with the 16.27 ka 3‰ excursion.

4. Discussion

4.1. SIMS versus micro-shaved data

Much of the variability in SIMS measurements is larger than the point-to-point reproducibility that is suggested by repeat measurements of SRM612 (±0.4–0.5‰ 2 s.d.) and suggests that the observed variability of O isotopes dominantly reflects changes in the isotopic composition of speleothem YT as opposed to analytical variability. As the SIMS data show substantially greater variability than the micro-shaved data, we conclude that the SIMS data resolve numerous events (with timescales of 20 years or less), which were averaged in the lower-resolution micro-shaved data. Furthermore, the SIMS measurements resolve the structure of the abrupt +2‰ isotopic shift, with the full shift taking place in 6 years and the majority (75%) of this transition occurring in just 1–2 years. Other features such as frequent 1–2‰ fluctuations of ca. 5 years duration (at 16.45, 16.40 and 16.37 ka) and a 3‰ excursion at 16.27 ka are also clear features in the SIMS $\delta^{18}O$ data. Interestingly, the 3‰ excursion was isotopically larger than the abrupt 16.07 ka isotopic shift, although in an opposite sense, and much shorter-lived. Large, reproducible shifts in SIMS $^{18}O/^{16}O$ measurements can occur when secondary ion optics are affected by variations in sample topography or interruption of electrical continuity due to sample cracks or Au-coat imperfections. No such

features occur on the surface of YT where the 3‰ excursion was measured and moreover, the sample mount had been lightly polished and recoated between measurement sessions 1.2 and 2.1 which both detect this feature. Furthermore, SRM612 measurements before, at and after this excursion indicate steady analytical conditions. The replication of this feature indicates that it is a natural feature and is a good example of how SIMS analyses can resolve short-lived features that are not resolvable in the micro-shaved data. The 3‰ excursion lasted only 5 years and is recorded in approximately 200 μm of growth, which would not be easily resolved with conventional methods.

The excellent agreement between $\delta^{18}O$ data where sessions 2.1 and 3.1 overlap suggests that the method of monitoring IMF drift by mounting SRM612 glass and speleothem in adjacent strips works well. Replacing SRM612 with a strip of an isotopically homogeneous carbonate standard could further improve this method by allowing the SIMS $\delta^{18}O$ data to be placed more accurately on the VPDB or VSMOW scale. The agreement between broad trends in the SIMS and micro-shaved data also suggests that the SIMS technique is valid, although over one section, 16.20–16.12 ka, agreement is poor and trends are antiphase. There is no clear reason for this disagreement and it cannot be explained by relatively poorer reproducibility of the SIMS data given that the trends in session 2.1 agree with those in session 1.2. The disagreement between SIMS and micro-shaved data may be due to sampling of different transects through the speleothem growth axis, however, the growth layers in the section of YT examined in this study appear to be near parallel.

4.2. Isotopic variations: short-lived fluctuations versus the 16.07 ka shift

Mean $\delta^{18}O$ values in the much longer micro-shaved $\delta^{18}O$ record are relatively constant ($\sim 6.0 \pm 0.3‰_{VPDB}$; 1 s.d.) for ~1000 years prior to the 16.07 ka event (Fig. 1B) at which point a major change in mean monsoon climate occurred marked by the 2‰ shift. Mean $\delta^{18}O$ then slowly relaxes back to the previous value of 6‰ and remains at this level for about 500 years, after which, $\delta^{18}O$ begins to steadily become more negative, marking the transition into the Bolling-Allerod period (Fig. 1B; Wang et al., 2001). The 2‰ shift at the 16.07 ka event itself is unidirectional and sharp and represents a shift or step in mean speleothem $\delta^{18}O$. The SIMS data has shown that this shift was complete in 6 years and that 75% of this transition took place in just 1–2 years. Superimposed over these trends before and after 16.07 ka is predominantly multi-decadal isotopic variation of typically 0.5–1.5‰ but as large as 3‰ (Fig. 6A, B). The 2‰ shift at 16.07 ka is clearly detected in micro-shaved data whereas these multi-decadal fluctuations, some of which are isotopically equivalent or greater, do not appear at all. The key difference between these fluctuations and the 16.07 ka event is that the $\delta^{18}O$ excursions of the former are short-lived (<10–20 years). By contrast, the 16.07 ka event marks a shift in mean $\delta^{18}O$ that persists for 500 years. Thus only features that alter mean inter-decadal $\delta^{18}O$ are detectable in the micro-shaved data.

4.3. The timing of the 16.07 ka event and North Atlantic H1

A Heinrich event occurs at the culmination of successively colder D–O cycles when major iceberg discharges occur into the North Atlantic, releasing a large volume of IRD and fresh water. Rapid warming, evident in the Greenland ice records, follows ice break-up (Bond et al., 1993; van Kreveld et al., 2000). The period of more positive $\delta^{18}O$ values at 16.07 ka and after is interpreted as a significantly different EASM occurring approximately at the same time as the North Atlantic H1 event (Wang et al., 2001). Exactly how the rapid 2‰ shift in the Hulu Cave record is temporally related to the sequence of events in the North Atlantic is not certain. Direct dating of the sediments containing IRD material is hampered by uncertainties in converting radiocarbon to calendar years during a period of anomalous deep water circulation (Bond et al., 1992, 1993 and see Hemming, 2004). The Greenland ice cores are annually resolved over this interval but H1 does not appear clearly in the GISP2 record (Fig. 1C). Bond et al. (1993) correlate H1 event IRD with a $\delta^{18}O$ minimum in GRIP at about 16.4 ka (uncertainty estimated to be at least ± several hundred years; Johnsen et al., 1992); however these features are not compared in detail, so that the GRIP interval referred to as H1 is not clear.

Wang et al. (2001) compare the entire Hulu Cave composite $\delta^{18}O$ record (75–11 ka) and GISP2, and judge the isotopic relationship to be inverse: Greenland cooling ($\delta^{18}O$ more negative) coincides with more positive $\delta^{18}O$ values (e.g. a reduction in the EASM) in the speleothem monsoon record. This relationship between Greenland cooling and a less intense EASM is consistent with other East Asian paleo records (e.g. Wang and Sarnthein, 1999; An, 2000). However, it is notable that the isotopic trends differ in their rate of transition. Greenland cooling is gradual, whilst 75% of the 16.07 ka isotopic shift at Hulu Cave occurs in 1–2 years. Thus, in terms of rate, the isotopic transition at Hulu Cave is more similar to the abrupt terminal warming phase in the D–O cycles,

described to have taken place in "several decades or less" (Dansgaard et al., 1993). Of course this similarity may be coincidental since a shutdown in the global THC has been shown to provoke rapid climatic changes outside of the North Atlantic. However, the climatic link with respect to both timing and processes remains to be established.

4.4. Possible links between the North Atlantic and the 16.07 ka monsoon event

Several possible climatic links between the North Atlantic and the East Asian monsoon have been proposed in previous studies. These include the effect of Greenland cooling on both high latitude westerly wind strength and northern anticyclones which affect atmospheric pressure gradients across the Northern Hemisphere (Porter and An, 1995; Wang and Sarnthein, 1999; An, 2000). These interpretations primarily involve strengthening the winter relative to the summer monsoons. A shift in the ITCZ would impact the EASM more directly. Global climate model simulations (Dong and Sutton, 2002; Chiang et al., 2003; Chiang and Bitz, 2005; Zhang and Delworth, 2005) demonstrate a southward shift in the ITCZ in response to increased ice cover and lowered ocean heat transport in the high northern latitudes. Two studies included the Pacific sector and involve either communication between the Atlantic and Pacific Oceans via ENSO-type processes (Zhang and Delworth, 2005), or meridional communication directly across the Pacific (via evaporative cooling from strengthened northeast trades; Chiang and Bitz, 2005). Chiang and Bitz (2005) also point out that a more southerly ITCZ results in a strengthening of the descending arm of the Northern Hemisphere Hadley cell which could intensify and/or expand the subtropical western Pacific High (SWPH). The march of the summer monsoonal rainband across East Asia is critically dependent on the strength and western extent of the SWPH (Chang et al., 2000a,b; Wang et al., 2000; Lim et al., 2002). Thus it is plausible that either of the model scenarios discussed would affect rainfall $\delta^{18}O$ at Hulu Cave. Moreover, it is tempting to try to explain the rapid +2‰ shift in terms of a shift in the SWPH since SWPH anomalies develop in a matter of months and this could provide a possible mechanism for the rapid 1–2 year change in the EASM.

However, in terms of the instrumental record, SWPH anomalies have an ambiguous effect on the EASM (Chang et al., 2000a,b). A more stronger and more westward extending SWPH can either decrease or increase rainfall depending on whether a site is located underneath the anticyclone or at its northwestern margin where baroclinity and moisture convergence are greatest. The ambiguous effects of large-scale atmospheric circulation anomalies on the EASM no doubt contributes to the complex spatial relationship between rainfall amount and $\delta^{18}O$ in East Asia that has been discussed by Johnsen and Ingram (2004). Thus it is difficult to predict whether mechanisms discussed might have produced the observed isotopic shift at 16.07 ka in the Hulu Cave record. Because of this complexity, future investigations of the relationship between rapid climate events in the North Atlantic and the EASM could benefit from employing climate models fitted with hydrological isotopic tracers. Such experiments may help to realise the isotopic effect of perturbing regional atmospheric circulation patterns by shifting the ITCZ or otherwise.

4.5. The 16.07 ka event versus other isotopic fluctuations

The 16.07 ka abrupt shift is equivalent, at least isotopically, to other non-Heinrich correlated climate fluctuations observed in the speleothem record suggesting that the 16.07 ka isotopic shift is more remarkable for its persistence in the monsoon record rather than its magnitude. Whether isotopic magnitude indicates that the climatic manifestation of the H1 event in East Asia (in terms of rainfall amount and/or moisture source) and these shorter events were similar is uncertain as a number of climatic scenarios could result in the same $\delta^{18}O$ value. The Hulu Cave $\delta^{18}O$ record is a robust recorder of rainfall $\delta^{18}O$ (Wang et al., 2001) but interpreting the EASM $\delta^{18}O$ signal is complicated, as discussed. The rise in speleothem Mg after the 16.07 ka is not abrupt nor is it the highest in the record, but a rise in speleothem Mg, albeit relatively small, following the +2‰ $\delta^{18}O$ shift is consistent with a drier interval as interpreted by Wang et al. (2001). The similar wavelengths of Mg and $\delta^{18}O$ fluctuations elsewhere in the record suggest these short-lived $\delta^{18}O$ fluctuations also reflect varying amounts of local rainfall. However, the absence of any obvious rapid shift in Mg at 16.07 ka suggests the abrupt +2‰ shift at 16.07 ka may reflect a more integrated rainfall isotopic signal whilst the shorter-lived variation may reflect more local rainfall changes. That is, the rapid +2‰ shift reflects more complex isotopic changes from moisture source to site rather than just a local "amount effect" signal.

5. Conclusions

SIMS $\delta^{18}O$ data were used to increase the temporal resolution of the Hulu Cave record at least tenfold over the interval coinciding with the North Atlantic H1 event.

The SIMS $\delta^{18}O$ data reveals the 16.07 ka event at Hulu Cave is dominated by a +1.5‰ shift in 1–2 years and an overall 2‰ rise in 6 years. SIMS $\delta^{18}O$ data also reveal that the 2‰ shift at 16.07 ka was not larger than other variation measured before or after.

Heinrich events are dominant features in the Wang et al. (2001) record and are detectable by analyses of micro-shaved intervals because their impact on the EASM is relatively long-lived (approximately 500 years). SIMS $\delta^{18}O$ data shows that the Hulu Cave record is frequently punctuated by isotopic fluctuations of similar magnitude but of much shorter duration. These fluctuations are interpreted to represent more local rainfall changes while the +2‰ shift represents a rapid change in the underlying $\delta^{18}O$ mean driven by more complex and persistent processes that are maintained for 500 years.

The comparison of SIMS and micro-shaved $\delta^{18}O$ data highlights the strengths and weaknesses of both methods, in terms of precision and accuracy of $\delta^{18}O$ and in terms of the spatial and temporal resolution. SIMS O isotope analyses of speleothems are capable of achieving much higher spatial and hence temporal resolution, however, owing to the difficulties of standardizing SIMS analyses, they are best adopted for investigating small windows of data containing relatively large $\delta^{18}O$ variations. Monitoring for IMF drift and geometric effects requires that regular measurements are made using an isotopically homogeneous standard material mounted as close as possible to the speleothem section. In this study, after correcting for drift with closely interspersed reference material (SRM612) analyses, we estimate an overall point-to-point reproducibility of ±0.4–0.5‰ (2 s.d.) for individual speleothem spot measurements. The future development of an isotopically homogeneous carbonate standard that could be cut into fine strips would reduce the need to rely on conventional data to correct the analyses, but accuracy would still be limited to the overall precision of SIMS analysis.

Acknowledgements

We thank Erica Hendy, John Chappell, Ian Williams and P.K. Rustomji for helpful discussion; Ian Fairchild and John Craven for constructive reviews; PKR and H. Zhou for performing some of the SIMS analyses; T Kunihiro, G. Jarzebinski and O. Lovera for technical assistance. P.C. Treble and SIMS measurements were funded by the USA Department of Energy grant DE-FG-03-89ER14049 and the instrumentation and facilities of NSF grant EAR-0113563.

References

An, Z.S., 2000. The history and variability of the East Asian paleomonsoon climate. Quaternary Science Reviews 19 (1–5), 171–187.

Araguas-Araguas, L., Froehlich, K., Rozanski, K., 1998. Stable isotope composition of precipitation over southeast Asia. Journal of Geophysical Research 102 (D22), 28721–28742.

Bond, G., et al., 1992. Evidence for massive discharges of icebergs into the North Atlantic Ocean during the last glacial period. Nature 360, 245–249.

Bond, G., Broecker, W.S., Johnsen, S., McManus, J.F., Labeyrie, L., Jouzel, J., Bonani, G., 1993. Correlations between climate records from North Atlantic sediments and Greenland ice. Nature 365, 143–147.

Broecker, W.S., 2003. Does the trigger for abrupt climate change reside in the ocean or in the atmosphere. Science 300, 1519–1522.

Burns, S.J., Fleitmann, D., Matter, A., Kramers, J., Al-Subbary, A.A., 2003. Indian Ocean climate and an absolute chronology over Dansgaard/Oeschger events 9 to 13. Science 301, 1365–1367.

Chang, C.-P., Zhang, Y., Li, T., 2000a. Interannual and interdecadal variations of the East Asian summer monsoon and tropical Pacific SSTs. Part I: Roles of the subtropical ridge. Journal of Climate 13, 4310–4325.

Chang, C.-P., Zhang, Y., Li, T., 2000b. Interannual and interdecadal variations of the East Asian summer monsoon and tropical Pacific SSTs. Part II: Meridional structure of the monsoon. Journal of Climate 13, 4326–4340.

Chiang, J.C.H., Bitz, C.M., 2005. Influence of high latitude ice cover on the marine Intertropical Convergence Zone. Climate Dynamics. doi:10.1007/s00382-005-0040-5.

Chiang, J.C.H., Biasutti, M., Battisti, D.S., 2003. Sensitivity of the Atlantic Intertropical Convergence Zone to Last Glacial maximum boundary conditions. Paleoceanography 18 (4), 1–18. doi:10.1029/2003PA000916.

Coplen, T.B., 1988. Normalization of oxygen and hydrogen isotope data. Chemical Geology 72 (4), 293–297.

Cortijo, E., Yiou, P., Labeyrie, L.C.M., 1995. Sedimentary record of rapid climatic variability in the North Atlantic Ocean during the last glacial cycle. Paleoceanography 10, 911–926.

Dansgaard, W., Johnsen, S., Clausen, H., Dahl-Jensen, D., Gundestrup, N., Hammer, C., Hvidberg, C., Steffensen, J., Sveinbjornsdottir, A., Jouzel, J., Bond, G., 1993. Evidence for general instability of past climate from a 250-kyr ice-core record. Nature 364, 218–220.

Dong, B.W., Sutton, R.T., 2002. Adjustment of the coupled ocean-atmosphere system to a sudden change in the thermohaline circulation. Geophysical Research Letters 29 (15), 1728.

Domrös, M., Gongbing, P., 1988. The Climate of China. Springer-Verlag, Berlin. 360pp.

Frappier, A., Sahagian, D., Gonzalez, L.A., Carpenter, S.J., 2002. El Niño events recorded by stalagmite carbon isotopes. Science 298, 565.

Fairchild, I.J., Smith, C.L., Baker, A., Fuller, L., Spotl, C., Mattey, D., McDermott, F., EIMF, 2006. Modification and preservation of environmental signals in speleothems. Earth Science Reviews 75, 105–153.

Genty, D., Blamart, D., Ouahdi, R., Gilmour, M., Baker, A., Jouzel, J., Van-Exter, S., 2003. Precise dating of Dansgaard–Oeschger climate oscillations in western Europe from stalagmite data. Nature 421, 833–837.

Grimm, E.C., Jacobson, G.L., Watts, W.A., Hansen, B.C.S., Maasch, K.A., 1993. A 50,000-year record of climate and oscillations from

Florida and its temporal connection with the Heinrich events. Science 261, 198–201.
GRIP (Greenland Ice-Core Project) Members, 1993. Climate instability during the last interglacial period recorded in the GRIP ice core. Nature 364, 203–207.
Grootes, P.M., Stuiver, M., White, J.W.C., Johnsen, S.J., Jouzel, J., 1993. Comparison of oxygen isotope records from the GISP2 and GRIP Greenland ice cores. Nature 366, 552–554.
Heinrich, H., 1988. Origin and consequences of cyclic ice rafting in the northeast Atlantic Ocean during the past 130,000 years. Quaternary Research 29, 142–152.
Hemming, S.R., 2004. Heinrich events: Massive late Pleistocene detritus layers of the North Atlantic and their global climate imprint. Review of Geophysics 42. doi:10.1016/2003RG000128.
Hendy, C., Wilson, A., 1968. Palaeoclimatic data from speleothems. Nature 219, 48–51.
Hendy, I.L., Kennett, J.P., 2000. Dansgaard-Oeschger cycles and the California Current System: planktonic foraminiferal response to rapid climate change in Santa Barbara Basin, Ocean Drilling Program hole 893A. Paleoceanography 15 (1), 30–42.
IAEA/WMO, 2001. Global Network of Isotopes in Precipitation. The GNIP Database. Accessible at: http://isohis.iaea.org.
Ireland, T.R., 1995. Ion microprobe mass spectrometry: techniques and applications in cosmochemistry, geochemistry and geochronology. Advances in Analytical Geochemistry 2, 1–118.
Johnsen, K.R., Ingram, B.L., 2004. Spatial and temporal variability in the stable isotope systematics of modern precipitation in China: implications for paleoclimate reconstructions. Earth and Planetary Science Letters 220, 365–377.
Johnsen, S.J., Clausen, H.B., Dansgaard, W., Fuhrer, K., Gundestrup, N., Hammer, C.U., Iversen, P., Jouzel, J., Stauffer, B., Steffensen, J.P., 1992. Irregular glacial interstadials recorded in a New Greenland ice core. Nature 359 (6393), 311–313.
Kasemann, S., Meixner, A., Rocholl, A., Vennemann, T., Rosner, M., Schmitt, A.K., Wiedenbeck, M., 2001. Boron and oxygen isotopic composition of certified reference materials NIST SRM610/612 and reference materials JB-2 and JR-2. Geostandard Newsletters 25 (2), 405–416.
Kendall, A.C., Broughton, P.L., 1978. Origin of fabrics in speleothems composed of columnar calcite crystals. Journal of Sedimentary Petrology 48, 519–538.
Kolodny, Y., Bar-Matthews, M., Ayalon, A., McKeegan, K.D., 2003. A high spatial resolution $\delta^{18}O$ profile of a speleothem using an ion-microprobe. Chemical Geology 197, 21–28.
Lim, Y., Kim, K., Lee, H., 2002. Temporal and spatial evolution of the Asian Summer Monsoon in the seasonal cycle of synoptic fields. Journal of Climate 15, 3630–3644.
McManus, J.F., Francois, R., Gherardi, J.M., Keigwin, L.D., Brown-Leger, S., 2004. Collapse and rapid resumption of Atlantic meridional circulation linked to deglacial climate changes. Nature 428 (6985), 834–837.
Porter, S.C., An, Z.S., 1995. Correlation between climate events in the North Atlatic and China during the last glaciation. Nature 375, 305–308.
Schuhmacher, M.F.F., de Chambost, E., 2004. Achieving high reproducibility isotope ratios with the Cameca IMS 1270 in the multicollection mode. Applied Surface Science 231–232, 878–882.
Spötl, C., Mangini, A., 2002. Stalagmite from the Austrian Alps reveals Dansgaard–Oeschger events during isotope stage 3: Implications for the absolute chronology of Greenland ice cores. Earth and Planetary Science Letters 6356, 1–12.
Stott, L., Poulsen, C., Lund, S., Thurnell, R., 2002. Super ENSO and global climate oscillations at millennial time scales. Science 297, 222–226.
Treble, P., Shelley, J.M.G., Chappell, J., 2003. Comparison of high-resolution sub-annual records of trace elements in a modern (1911–1992) speleothem with instrumental climate data from southwest Australia. Earth and Planetary Science Letters 216, 141–153.
Treble, P.C., Chappell, J., Gagan, M.K., McKeegan, K.D., Harrison, T.M., 2005a. In situ measurement of seasonal $\delta^{18}O$ variations and analysis of isotopic trends in a modern speleothem from southwest Australia. Earth and Planetary Science Letters 233, 17–32.
Treble, P.C., Chappell, J., Shelley, J.M.G., 2005b. Complex speleothem growth processes revealed by trace element mapping and scanning electron microscopy of annual layers. Geochimica et Cosmochimica Acta 69, 4855–4863.
Valley, J.W., Graham, C.M., 1991. Ion microprobe analysis of oxygen isotope ratios in granulite facies magnetites: diffusive exchange as a guide to cooling history. Contributions to Mineralogy and Petrology 109, 38–52.
Valley, J.W., Graham, C.M., Harte, B., Eiler, J.M., Kinny, P.D., 1998. Ion microprobe analysis of oxygen, carbon and hydrogen isotopes. In: McKibben, M.A., Shanks, W.C., Ridley, W.I. (Eds.), Applications of microanalytical techniques to understanding mineralizing processes. Reviews in Economic Geology, vol. 7. Society of Economic Geologists, Littleton, CO, pp. 73–98.
van Kreveld, S., Sarnthein, M., Erlenkeuser, H., Grootes, P., Jung, S., Nadeau, M.J., Pflaumann, U., Voelker, A., 2000. Potential links between surging ice sheets, circulation changes, and the Dansgaard–Oeschger cycles in the Irminger Sea. Paleoceanography 15 (4), 425–442.
Wang, L., Sarnthein, M., 1999. Long-/short-term variations of monsoon climate and its teleconnection to global change. In: Abrantes, Mix (Eds.), Reconstructing Ocean History: A Window Into the Future. Kluwer Academic, New York, pp. 57–71.
Wang, B., Wu, R., Fu, X., 2000. Pacific-East Asian teleconnection: How does ENSO affect East Asian climate? Journal of Climate 13, 1517–1536.
Wang, Y.J., Cheng, H., Edwards, R.L., An, Z.S., Wu, J.Y., Shen, C.C., Dorale, J.A., 2001. A high-resolution absolute dated late Pleistocene monsoon record from Hulu Cave, China. Science 294, 2345–2348.
Wang, X.F., Auler, A.S., Edwards, R.L., Cheng, H., Cristalli, P.S., Smart, P.L., Richards, D.A., Shen, C.C., 2004. Wet periods in northeastern Brazil over the past 210 kyr linked to distant climate anomalies. Nature 432 (7018), 740–743.
Yuan, D., Cheng, H., Edwards, R.L., Dykoski, C.A., Kelly, M.J., Zhang, M., 2004. Timing, duration and transitions of the Last Interglacial Asian Monsoon. Science 304, 575–578.
Zhang, R., Delworth, T.L., 2005. Simulated tropical response to a substantial weakening of the Atlantic thermohaline circulation. Journal of Climate 18, 1853–1860.